Crown-Like Baffle System against Rock Avalanches: Energy Dissipation Mechanism and Numerical Verification

Yu Huang [*1, 2], **Hao Shi**[1], **Bei Zhang**[2]

1. *Department of Geotechnical Engineering, College of Civil Engineering, Tongji University, Shanghai* 200092, *China*
2. *Key Laboratory of Geotechnical and Underground Engineering of the Ministry of Education,*
Tongji University, Shanghai 200092, *China*

Yu Huang: https://orcid.org/0000-0002-9935-7717

ABSTRACT: In mountainous areas, rock avalanches swarm downslope leading to large impact forces on structures. Baffle systems are usually set up in torrent channels to dissipate the flow energy and reduce the destructive effects. In this paper, a crown-like baffle system is proposed to better dissipate the flow energy. The energy dissipation mechanism of this system was investigated based on DEM. The results reveal more than 90% of the kinetic energy of the granular flow was dissipated by particle-particle interaction. Two effects, the impedance effect and the deflection effect, were identified. The influence of these effects leads to the formation and growth of cushions behind the baffles, and these cushions enhance the particle-particle interaction. Two crown-like baffle systems were compared with a conventional baffle system based on the typical avalanche model. The results reveal the cumulative residual kinetic energy of the crown-like baffle system with square baffles decreased by 18.75% with the same concrete consumption as the conventional baffle system. For the crown-like baffle system with triangular baffles, the cumulative residual kinetic energy decreased by 6.22% with 83.94% of the concrete consumption of the conventional baffle system. Hence, the proposed baffle system is more cost-effective compared with the conventional baffle system.
KEY WORDS: rock avalanches, new baffle system, energy dissipation, discrete element method, engineering geology.

0 INTRODUCTION

A rock avalanche is an extremely rapid, massive, flow-like motion of fragmented rock from a large rockslide or rock fall (Hungr et al., 2001). Because of their extremely high mobility and enormous volume, rock avalanches often lead to tremendous damage downstream. For example, the 2.5 M m³ Punta Thurwieser rock avalanche occurred in the Italian Central Alps on September 18th, 2004, and traveled over 2.9 km from the source (Sosio et al., 2008). The Chediguan Bridge, located in Sichuan, China, collapsed due to falling rock collision in 2009, resulting in three people being killed and a further 12 being injured (Zhang et al., 2020). On 14th August, 2019, a rapid rock avalanche led to seventeen deaths and destroyed a 70-m-long section of a railway line in Sichuan Province, China (Zhao et al., 2020).

To mitigate the subsequent destructive effects caused by rock avalanches, many studies have put great effort into consolidating the resistance of building structures to disasters (Tiago and Júlio, 2010). However, the reinforcement of existing buildings requires substantial resources. Therefore, countermeasures such as protective dykes, silt dams, and baffle systems, are often installed in torrent channels (Goodwin and Choi, 2020; Ng et al., 2015; Mancarella and Hungr, 2010; Suda et al., 2009). Among these measures, the use of baffle systems is particularly effective in impeding the flow mobility of rock avalanches (Wang et al., 2020a). The function of a baffle system is to perturb the flow pattern and dissipate the flow energy through the interactions between the piles and gravel. The results obtained by flume experiments conducted by Ng et al. (2015) revealed that three rows of baffles can lead to the decrease of runout by 65% and decrease of frontal velocity by up to 57%. Additionally, baffle systems have the advantage of low construction cost and strong construction adaptability compared with other countermeasures (Wang et al., 2020a).

Because this structure has great application potential in disaster mitigation, it has attracted the attention of many studies. Flume experiments have been conducted to investigate the flow-baffle interaction mechanisms (Ng et al., 2015). In addition to physical modelling, numerical simulations can be conducted to investigate the interaction between granular flows and structures. Numerical methods based on continuum mechanics, such as the depth average technique (Fei et al., 2020), material particle method (Li et al., 2020), and arbitrary Lagrangian–Eulerian finite element method (Kwan et al., 2015), can perform reasonably well in estimating global quantities, such as the runout patterns and overall force in the soil-structure interaction. How-

ever, these methods cannot satisfactorily describe dynamic behaviour, such as shock waves (Khan et al., 2020), dead zones (Choi et al., 2015), and phase transition (Hu et al., 2015), when avalanches flow around an obstacle. The discrete element method (DEM) has been widely used to investigate the granular-structure interaction mechanism. By conducting a 3D DEM study, Huang et al. (2020) discovered that the flow-baffle interaction is controlled by the evolution of force chains. The DEM has also been used to investigate the effect of the configuration on the impact force that rock avalanches exert on baffle systems (Bi et al., 2019, 2018).

Although baffle systems can effectively dissipate the flow energy, there is still much room for improving the flow energy dissipation capability of such systems. The baffle system configuration greatly influences the impeding of the flow mobility of rock avalanches. Flume experiments have been conducted to investigate the influence of the baffle height, row number, and spacing between successive rows on the capacity of flow energy dissipation (Ng et al., 2015; Choi et al., 2014). Choi et al. (2015) investigated the effect of configuration on the energy dissipation of granular flow using the DEM. Several principles have been proposed to guide the design of baffle systems (Law et al., 2016). However, the shape of baffle systems can significantly affect the energy dissipation process. Based on flume modelling, three baffle system types have been investigated. The results reveal that arch-shaped baffle systems have the best energy dissipation capability among these three baffle system types (Wang et al., 2020a).

This paper proposes the concept of a crown-like baffle system. The energy dissipation mechanism and energy dissipation capacity of the proposed novel baffle system were investigated and verified using the DEM. In the rest of this paper, the theory of the DEM is first introduced. Then, a brief introduction on the layout of crown-like baffle systems is given, and the energy dissipation mechanism of this new baffle system is investigated using the DEM. A practical-scale numerical model is established to demonstrate the advantages of the new structure in terms of economic feasibility and energy dissipation capability. The results obtained by this study can be useful for improving the design of baffle systems.

1 DEM THEORY

The DEM is particularly promising for modelling rock avalanches (Mead and Cleary, 2015; Salciarini et al., 2010). In this paper, the 3D DEM code EDEM (DEM Solutions, 2020) was adopted to investigate the interaction between granular flow and a baffle system. In the DEM, the granular mass is considered as a group of individual bodies. The motion of the granular mass is modelled by solving Newton's equation of motion for each individual body. The total force and moment imposed to the particle i is expressed as follows

$$\vec{F}_i = m_i \frac{\mathrm{d}\vec{v}_i}{dt} = \sum_{j=1}^{n}(\overrightarrow{F_{ij}^n} + \overrightarrow{F_{ij}^t}) + \overrightarrow{F_i^b} \qquad (1)$$

$$\overrightarrow{M}_i = m_i \frac{\mathrm{d}\vec{\omega}_i}{dt} = \sum_{j=1}^{n}(\overrightarrow{M_{ij}^t} + \overrightarrow{M_{ij}^r}) \qquad (2)$$

The total force $\vec{F}_i$ is decomposed into the sum of the con-

tact force and body force $\overrightarrow{F_i^b}$. When two colliding bodies i and j undergo deformation, the contact force is decomposed into the normal force $\overrightarrow{F_{ij}^n}$ and tangential force $\overrightarrow{F_{ij}^t}$. The total moment comprises the sum of the tangential moment $\overrightarrow{M_{ij}^t}$ and roll moment $\overrightarrow{M_{ij}^r}$. Based on Newton's equation of motion, the total force is equal to the mass m_i multiplied by $\frac{\mathrm{d}\vec{v}_i}{\mathrm{d}t}$, and the total moment is equal to the mass m_i multiplied by $\frac{\mathrm{d}\vec{\omega}_i}{\mathrm{d}t}$, where $\vec{v}_i$ and $\vec{\omega}_i$ donate the translational and angular velocity of particle i, respectively.

The contact force is calculated using the Hertz-Mindlin (no slip) model, which has satisfactory numerical accuracy and computational efficiency (Jiang et al., 2018). The normal force is decomposed into an elastic force, F_n^e, for the elastic deformation of the particle, and a damping force, F_n^d, arising from the energy dissipation caused by viscous deformation.

$$F_n = F_n^e + F_n^d = \frac{4}{3}E^*\sqrt{R^*}\,\delta_n^{\frac{3}{2}} - 2\cdot\sqrt{\frac{5}{6}}\cdot\beta\cdot\sqrt{S_n m^* v_n^{rel}} \qquad (3)$$

Limited by Coulomb's law of friction, the tangential force is expressed as follows

$$F_t = \min\left\{F_t^e + F_t^d, \mu F_n\right\} = \min\left\{S_t \delta_t + \right.$$
$$\left. 2\cdot\sqrt{\frac{5}{6}}\cdot\beta\cdot\sqrt{S_t m^* v_t^{rel}}, \mu F_n\right\} \qquad (4)$$

where the normal stiffness S_n, tangential stiffness S_t, and β are expressed as follows

$$S_n = 2\cdot E^*\sqrt{R^*\delta_n} \qquad (5)$$

$$S_t = 8\cdot G^*\sqrt{R^*\delta_n} \qquad (6)$$

$$\beta = \frac{-ln^e}{\sqrt{ln^{2e} + \pi^2}} \qquad (7)$$

where E^* is the equivalent Young's Modulus; G^* is the equivalent shear modulus; R^* is the equivalent particle radius; m^* is the equivalent particle mass; v_n^{rel} and v_t^{rel} are the normal component and tangential component of the relative velocity, respectively; δ_n and δ_t are the normal overlap and tangential overlap, respectively; μ is the coefficient of static friction; e is the coefficient of restitution.

The rolling friction is implemented by applying torque to the contact surfaces, as follows

$$M^r = \mu_r F_n R_i \hat{\omega}_i \qquad (8)$$

where μ_r is the rolling friction coefficient; R_i is the distance between the contact point and the center of the particle; $\hat{\omega}_i$ is the unit angular velocity vector at the contact point.

2 LAYOUT OF CROWN-LIKE BAFFLE SYSTEM

Granular material is typical soft matter (van der Gucht, 2018) for which a small change can remarkably alter the state of the material (Daoud and Williams, 1999). This means that a reasonable baffle system design can greatly improve the sys-

tem's energy dissipation capacity. The influence of the baffle height, transverse blockage, row number, row spacing, and baffle shape on the energy dissipation capacity of a baffle system have been extensively investigated (Huang et al., 2020; Choi et al., 2014). Compared with ordinary shapes, such as the square and triangle, a structure with a curved surface (Fig. 1) always achieves better energy dissipation (Wang et al., 2020a; Choi et al., 2017; Ng et al., 2017). Under this condition, the particles collide with the structure at an oblique angle, and therefore the impact momentum of the structure decreases compared with the frontal impact. When the particles move along the arc, the flow direction of the particles changes and the flow path of the particles increases, which results in additional energy dissipation. Additionally, the structure retains some particles and a particle cushion is formed. This cushion can dissipate the energy of subsequent granular flow (Wang et al., 2020b) and may reduce the impact force in some cases (Choi et al., 2017). However, this structure is fragile on the brink of an arc and its construction is more difficult.

Inspired by the above-mentioned studies, a crown-like baffle system is proposed by changing the layout of a conventional baffle, as shown in Fig. 2. The design principles of this system are briefly as follows

(1) To simplify the design of the baffle system, the baffles are arranged along an arc, as shown in Fig. 2a, where O is the centre of arc AC, θ is the central angle of arc AC, and r is the radius of arc AC. Three square baffles form the design unit of the baffle system, which is referred to as the crown in this paper. These baffles are tangential to arc AC and horizontally symmetrical along the symmetry axis OB.

(2) In addition to square baffles, other baffle shapes, such as triangular baffles, can also be used in this baffle system. The baffle width is denoted as b and the silt size of the crown is denoted as s, as shown in Fig. 2b.

(3) In Fig. 2c, the crowns are lined up to form the row of a baffle system. To better guide the granular material flow along the arc of the crown, the symmetry axis OB may not be parallel to the flow direction. Here, γ is the deflection angle of the crown. The gap between two crowns is defined as g. An individual baffle can be installed between two crowns as a deflector.

(4) Transverse blockage is an important parameter in baffle design. According to the definition of transverse blockage (Ng et al., 2015), the equivalent transverse blockage T_b' is expressed as follows

$$T_b' = \left[1 - \frac{(\sum s + \sum g)}{W}\right] \times 100 \qquad (9)$$

3 ENERGY DISSIPATION MECHANISM OF CROWN-LIKE BAFFLE SYSTEM

3.1 DEM Model Program

Jiang and Towhata (2013) conducted a series of flume tests to investigate the interaction between dry granular flows and a rigid wall. In this study, the same flume model was adopted to investigate the energy dissipation mechanism of the crown-like baffle system. The configuration of the flume model is shown in Fig. 3. By comparing the final deposition and time evolution of the impact force obtained by the flume tests to those obtained by numerical simulation, Huang et al. (2020)

calibrated a set of DEM parameters based on experimental measurement (Jiang and Towhata, 2013) and numerical calculation results (Zhou et al., 2020; Jiang et al., 2018; Shen et al., 2018). The detailed input parameters are listed in Table 1.

The crown-like baffle system was set in the baffle system installation section; the vertical view of the baffle system is shown in Fig. 4. The baffle width was 1.75 cm. The design parameters of the crown are listed in Table 2. The equivalent transverse blockage was 40%, which is the upper blockage limit
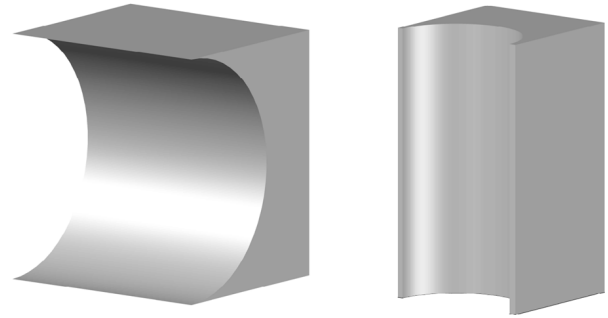

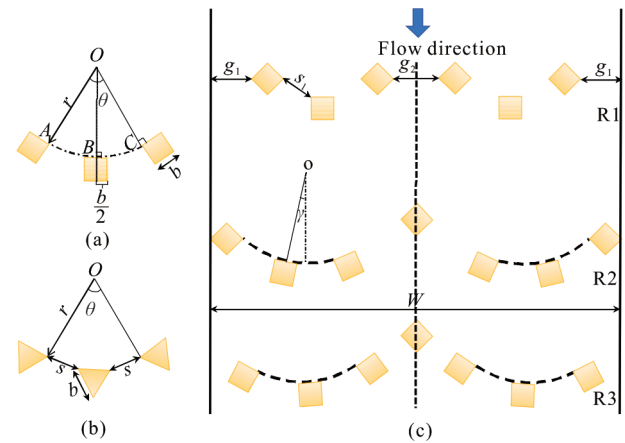**Figure 1.** Examples of curved structure (Wang et al., 2020a; Choi et al., 2017).

Figure 2. Layout of crown-like baffle system: (a) crown with square baffles; (b) crown with triangular baffles; (c) example of crown-like baffle system.
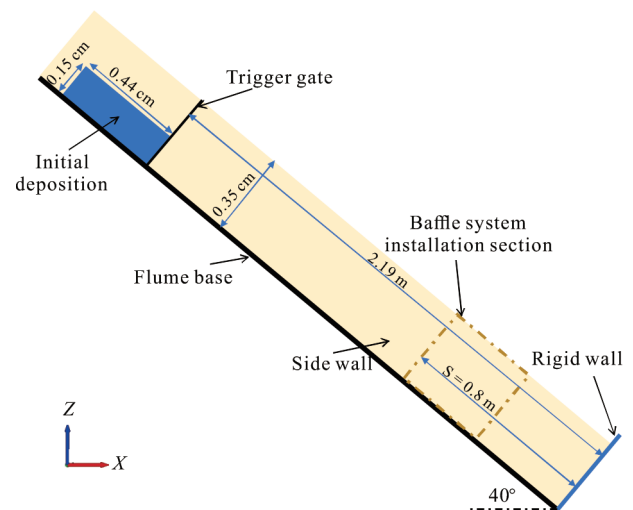

Figure 3. Configuration of flume model.

of the baffle system defined by Ng et al. (2014). To better elucidate the energy dissipation mechanism, granular overflow must be prevented. Therefore, the baffle height was set to 0.35 m. Three monitoring sections were set to better understand the energy dissipation mechanism and evaluate the energy dissipation capacity of the crown-like baffle system, as shown in Fig. 4.
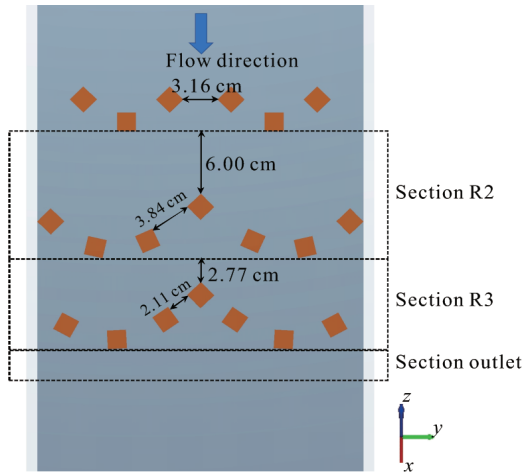

Figure 4. Vertical view of baffle system.

Table 1 Flume test simulation input parameters (Huang et al., 2020)

Material	DEM parameters	Value	Source
Particle	Density ρ_1 (kg/m³)	2 550	Limestone
	Poisson's ration υ_1	0.25	Limestone
	Elastic modulus E_1 (MPa)	100	Shen et al. (2018)
	Friction coefficient μ_1	1.33	Jiang and Towhata (2013)
	Rolling friction coefficient μ_{r1}	0.06	Calibration
Rigid wall	Density ρ_2 (kg/m³)	7 900	Steel material
	Poisson's ration υ_2	0.3	Steel material
	Elastic modulus E_2 (GPa)	200	Steel material
	Friction coefficient μ_2	0.384	Jiang and Towhata (2013)
	Rolling friction coefficient μ_{r2}	0.01	Zhou et al. (2020)
Flume base	Density ρ_3 (kg/m³)	7 900	Steel material
	Poisson's ration υ_3	0.3	Steel material
	Elastic modulus E_3 (GPa)	200	Steel material
	Friction coefficient μ_3	0.466	Jiang and Towhata (2013)
	Rolling friction coefficient μ_{r3}	0.01	Same with rigid wall
Side wall	Density ρ_4 (kg/m³)	7 900	Steel material
	Poisson's ration υ_4	0.3	Steel material
	Elastic modulus E_4 (GPa)	200	Steel material
	Friction coefficient μ_4	0.268	Jiang and Towhata (2013)
	Rolling friction coefficient μ_{r4}	0.01	Same with rigid wall
Restitution coefficient e		0.6	Jiang et al. (2018)

Table 2 Design parameters

Row number	r (cm)	θ (°)	γ (°)
R1	3.6	99	0
R2	6.5	61	12
R3	6.0	68	3

3.2 Numerical Simulation and Analysis of Results
3.2.1 Flow patterns

Figure 5 shows a series of vertical snapshots capturing the interaction of granular flow with the baffle system; the particles are coloured according to the velocity magnitude. Under the guidance of the baffle system, the flow direction of the particles changes dramatically. To show the change of the flow directions, the particles are displayed as vectors. The vector direction represents the velocity direction, while the vector length represents the velocity magnitude. The vector is coloured according to the component of velocity in the *y*-direction, as shown in Fig. 6.

After opening the trigger gate for 0.7 s, the flow front with an approach velocity of 3 m/s began to impact the first row (Fig. 5a). Seven granular jets formed through the gaps between the crowns and the silts within the crowns. Owing to the impedance effect of the crowns, there is an obvious speed difference between these granular jets. The granular jets that formed through the gaps between the crowns with higher flow velocity can be grouped together. The granular jets that formed through the silts within the crowns with lower flow velocity can be gathered into another group, as shown in Fig. 5b.

The flow directions of faster granular jets changed dramatically when they collided with the second row. The deflected jets began to move transversely and were deposited behind the baffles, as shown in Fig. 6b. The accumulated particles began to form cushions behind the crowns of the second row of the baffle system, as shown in Fig. 5*b*. Moreover, the slower granular jets flowed to the front of the second row of the baffle system and interacted with the second row and the cushions behind them.

The particles were further divided into six granular jets as they propagated past the second row. The granular jets of the second row were more dispersed compared with those of the first row, as shown in Figs. 5c, 6c. The dispersed granular flow was blocked by the third row of the staggered baffles. The arc of the crown caused the particles to gather in the centre of the crown and begin to form a cushion behind the third row.

Owing to the impedance effect and deflection effect of the baffle system, the particles were gradually deposited behind the baffles. The continuous accumulation of particles in the baffle installation section led to the gradual thickening of the cushions, as shown in Figs. 5d–5f, 6d–6f.

The granular flow became slow and steady since $t = 1.4$ s, as shown in Figs. 5g–5i. The space between the baffles was gradually occupied by the deposited particle. The transverse velocity of the particles gradually decreased, as shown in Figs. 6g–6i, which means that the deflection effect of the baffle system became increasingly weaker. The friction between the deposited particles and the subsequent granular flow led to the loss of kinetic energy.

3.2.2 Evolution of kinetic energy

Baffles are commonly installed in front of rigid barriers to dissipate the flow energy of granular flow (Bi et al., 2018; Law et al., 2016). The analysis of the energy evolution is important for understanding the energy dissipation mechanism of baffle systems. Moreover, the energy dissipation capacity is a crucial
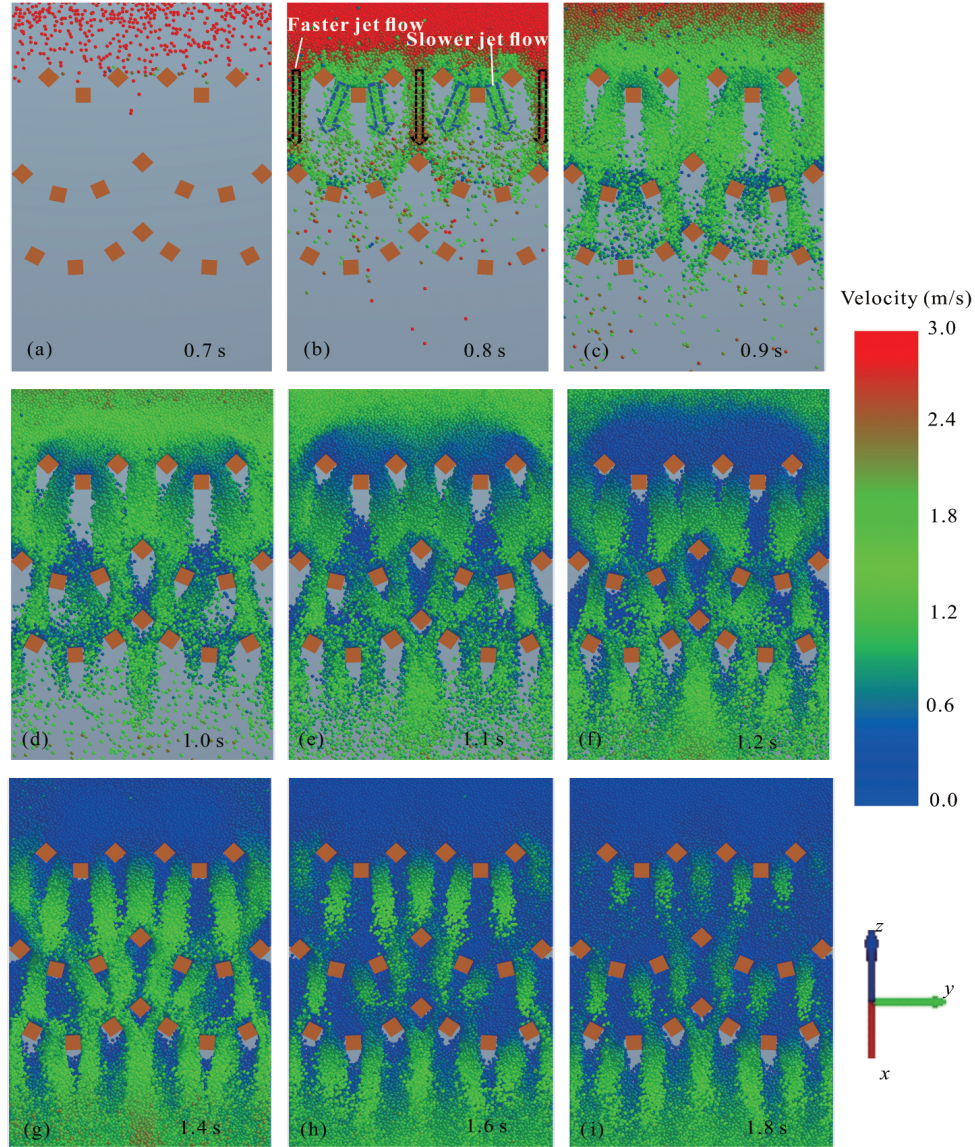
Figure 5. Progress of granular flow movement at different times.

metric for evaluating the performance of baffle systems. Hence, the kinetic energy evolution of the granular flow is thoroughly discussed in this section.

Figure 7 shows the evaluation of the kinetic energy of particles encompassed in the monitoring section outlet. The kinetic energy of the particles encompassed in the monitoring section at a given time is calculated as follows

$$E_K^t = \sum_{i=1}^n \frac{1}{2} m_i |v_i|^2 + \sum_{i=1}^n \frac{1}{2} I_i |\omega_i|^2 \qquad (10)$$

Here, n is the total number of particles in the monitoring section; the first term represents the translation kinetic energy of the particles, while the second term represents the rotational kinetic energy of the particles.

As shown in Fig. 7, the kinetic energy reached 2.78 J at 1.1 s in the case of free flow (without the baffle). Compared with free flow, the kinetic energy of the monitoring section was significantly lower when the baffle was installed. The kinetic energy reached 0.23 J at 1.3 s when the baffle was installed. The kinetic energy reduction ratio is used to evaluate the dissi-

pation capacity of the baffle system. The reduction of kinetic energy is defined as follows

$$E = \sum_{t=0}^{t=\text{end}} E_{K\_F}^t - \sum_{t=0}^{t=\text{end}} E_{K\_B}^t \qquad (11)$$

where the first term represents the cumulative kinetic energy in the case of free flow, and the second term represents the cumulative kinetic energy when the baffle is installed. In the case of free flow, the cumulative kinetic energy was 13.76 J. When the baffle was installed, the cumulative kinetic energy was 1.22 J. Therefore, $E = 12.54$ J, which means that the kinetic energy was reduced by 91% as a result of installing the baffle system.

The kinetic energy reduction caused by the installation of the baffle system can be divided into two parts: particle-particle interaction and particle-baffle interaction. The kinetic energy of the particles that dissipate owing to the inelastic contact between the particles and the baffles is expressed as follows

$$E_{\text{ine}}^t = \sum_{i=1}^k (E_{\text{ine}}^n + E_{\text{ine}}^s + E_{\text{ine}}^r) \qquad (12)$$

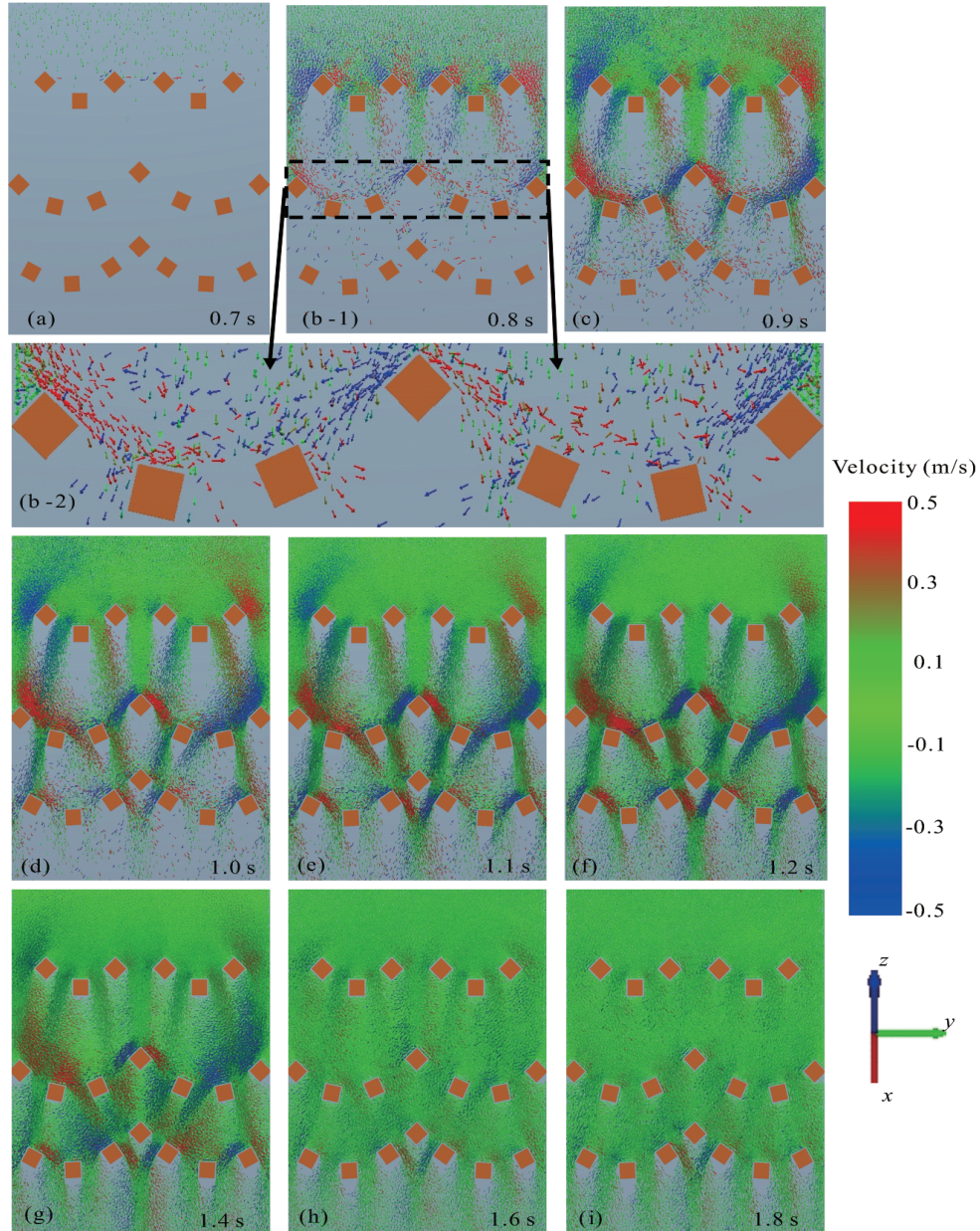where k is the number of particles interacting with the baffle,

Figure 6. Velocity vectors of particles at different times.

E_{ine}^n is the energy dissipation caused by normal collision, E_{ine}^s is the energy dissipation caused by tangential shear, and E_{ine}^r is the energy dissipation caused by rolling friction. To quantitatively evaluate the contribution of the particle-baffle interaction, the cumulative kinetic energy dissipation ($\sum E_{ine}^t$) was calculated during the simulation. Notably, $\sum E_{ine}^t$=0.42 J, which only 3.3% of the kinetic energy reduction E. This result reveals that the particle-particle interaction is the main approach for dissipating the kinetic energy of particles. Therefore, the function of a baffle system is to enhance the particle-particle interaction.

3.2.3 Evolution of force chain

Force chain is a fundamental approach for investigating the behaviour of granular material from a meso viewpoint. Zhang et al. (2017) have pointed out that force chains play an important role in governing the microstructure of granular ma-

terial, and the number of force chains is correlated with the energy dissipation inside the granular material. In this study, the force chain was considered to qualitatively investigate the energy dissipation mechanism. The evolution of the force chains is shown in Fig. 8.

When the granular flow propagated in front of the first row, the force chains were very sparse, as shown in Fig. 8a. This indicates that the granular flow was in the dilute condition under which the particles interacted through binary and instantaneous collisions (Delannay et al., 2017). With the continuous impact of subsequent granular flow onto the first row of baffles, the force chains behind the first row became denser, as shown in Fig. 8b. When the particles flowed through the crown slits, the arches that formed between the baffles led to the jamming of particles, as shown in Fig. 8c. The interaction of subsequent incoming flows with arches led to the deceleration of the
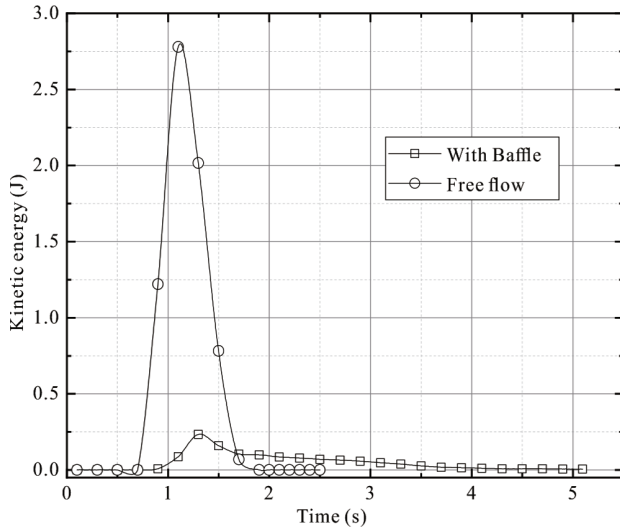
Figure 7. Evolution of kinetic energy of particles encompassed in monitoring section outlet.

granular jets. The flow energy was partly dissipated by the constant destruction and regeneration of the arches. The width of the openings has a strong influence on particle jamming, and a narrow opening is more conducive to the occurrence of the jamming phenomenon (Hu et al., 2015). Therefore, granular jets form through the gaps between crowns with a wider flow path, and the reduced probability of jamming leads to a higher flow velocity. Owing to the deflection effect of the baffle sys-

tem, faster granular jets flow along the arcs of the second row and force chains appear behind the second row, as shown in Fig. 8d. The force networks behind the baffles indicate the formation of a particle cushion behind the second row.

As the particles propagate past the first row, the force networks become increasingly denser. The particles that continuously flow through the gaps between the crowns help the growth of the cushion behind the second row. Additionally, the granular jets flowing along the particle cushions enhance the energy dissipation. Once the particle cushions are formed, the granular jets flowing through the crown slits collide with the cushions instead of directly colliding with the baffles, as shown as Fig. 8h. This mechanism helps the blockage of particles and enhances the particle-particle interaction. Moreover, force chains begin to appear behind the third row, as shown in Fig. 8f. The particles pass the second row as the cushions grow behind the second row. As shown in Fig. 8g, continuous force networks appear behind the third row, which indicates the formation of cushions behind the third row.

The particles continuously flow into the baffle installation section. The force chains gradually occupy the space between the baffles, as shown in Figs. 8i–8l. The complex force networks shown in Fig. 8l indicate that the granular flow is in the dense condition, under which the response of the granular flow is governed by the enduring contact among the particles and the entire force networks have to be continuously rearranged (Delannay et al., 2017). The rearrangement of the force networks leads to the dissipation of flow energy.
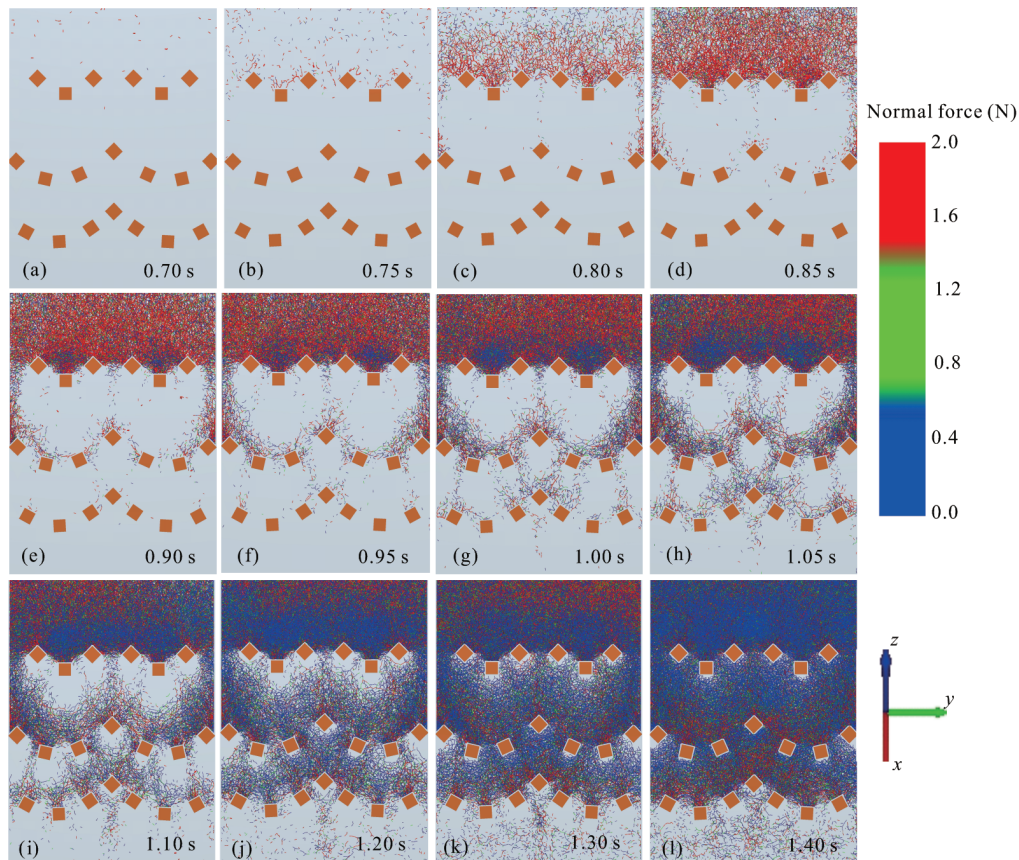

Figure 8. Force chains at different times.

3.2.4   Evolution of average coordination number

The amount of contact among the particles is another fundamental concept for investigating the behavior of granular material from a meso viewpoint. A larger amount of contact among the particles results in more effective restriction on the particle movement and reduces the rotation of particles, which leads to greater bulk stiffness (Matthew, 2017). The average coordination number theoretically reflects the average number of contacts per particle in the rectangular monitoring section, and is expressed as follows

$$C_0 = \frac{1}{N_{cell}} \sum_{i=1}^{N_{cell}} n_{co,i} \tag{13}$$

where C_0 is the average coordination number, $n_{co,i}$ is the contact amount of the ith particle in the monitoring section, and N_{cell} is the total number of particles in the monitoring section. In this section, the evolution of the average coordination number in monitoring sections R2 and R3 is investigated as shown in Fig. 9.

As can be seen in Fig. 9, C_0 in monitoring section R2 and C_0 in monitoring section R3 exhibit the same evolutionary trend. As the time increases, each C_0 evolution line increases to a certain extent, and there are two turning points in each C_0 evolution line. By comparing Figs. 5, 8, it can be seen that these turning points have an obvious physical meaning. Turning point *N* indicates the time when the cushion formation is completed, and turning point *M* indicates the time when the space between the rows has been completely occupied by particles.

The two turning points divide the C_0 evolution line into three parts. This indicates that three stages exist during the granular flow interaction with the baffle system. In this paper, these stages are defined as the cushion formation stage, cushion growth stage, and steady flow stage. The cushion formation stage of R2 was shorter than that of R3, which coordinated with the faster granular jets of R1 as shown in Fig. 5. Because the space between R1 and R2 was larger than that between R2 and R3, the cushion growth stage was longer in monitoring section R2. The influence of the obstruction effect of R3 on monitoring section R2 resulted in a higher C_0 in monitoring section R2 compared with that in monitoring section R2 at the steady flow stage.
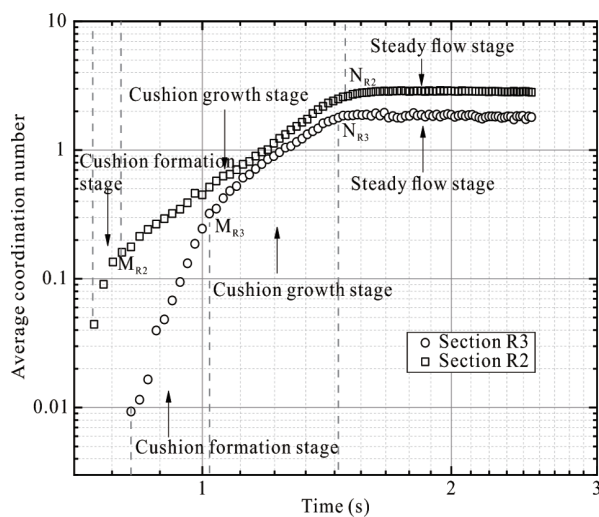

Figure 9. Evolution of average coordination number.

3.3   Energy Dissipation Mechanism

For researchers and engineers, understanding the energy dissipation mechanism of a baffle system is fundamental for designing baffle systems. Based on the above-mentioned numerical simulation results, this section discusses the energy dissipation mechanism of the crown-like baffle system in detail.

The investigation of the interaction mechanism of traditional baffle systems has confirmed that particle-particle interaction is the main energy dissipation mechanism (Huang et al., 2020). Based on the energy analysis results, more than 90% of the granular flow's kinetic energy is dissipated by particle-particle interaction and only a small part of kinetic energy is dissipated by particle-baffle interaction. In the same manner as the traditional baffle system, the function of the crown-like system is to enhance the particle-particle interaction.

The impedance effect and deflection effect occur when particles interact with the crowns. Granular flows collide with baffles at different incident angles. When particles collide with baffles at small incident angles, the reflective forces generated from the baffles support the blocked particles to form arches between the baffles, as shown in Fig. 8c. The impedance effect is caused by the arches that form between the baffles. When an arch is formed between the baffles, the granular flow is in a jammed state. The interaction between the subsequent incoming granular flow with arches leads to the deceleration or halting of the particles. The crowns can be considered as a type of barrier when the impedance effect of the crown exerts great influence on the particles. The deflection effect is caused by the unique layout of the crown. When the granular flow collides with the baffle at a large incident angle, the granular flow is deflected and flows parallel to the baffles. Then, the deflected granular flow tends to flow along the arc of the crown, as shown in Fig. 6d. The crowns can be considered as a type of deflecting dam when the deflection effect of the crown exerts great influence on the particles.

The first row of the baffle system mainly serves as a type of barrier. Under the impedance effect, the force chains behind the first row of the baffle system rapidly become denser. The interaction between the subsequent incoming granular flows with arches leads to the deceleration of the granular jets that form through the silts within the crowns.

Based on the evolution of the average coordination number, the interaction process during the passage of granular flows through the second and the third rows of the baffle system can be divided into three stages. Notably, the crowns play different roles at different stages of the interaction process.

At the cushion formation stage, the granular jets with higher kinetic energy are deflected to flow parallel to the baffles and then flow across the baffles, as shown in Fig. 6c. Because the flow direction of the granular jets is approximately vertical to the openings between the baffles, the particles gather behind the crowns and force chains gradually appear behind the crowns, as shown in Fig. 8d. The low average coordination number indicates that the granular flows are in a dilute state at this stage. For dilute flow, particle-particle interactions play a minor role (Delannay et al., 2017), and the kinetic energy of the granular jets is seldom dissipated at this stage. Moreover, during this stage, the crowns serve as a type of deflecting dam.

At the cushion growth stage, the particles that continuously flow through the gaps between the crowns help the cushion growth under the deflecting effect of the crowns. Thicker cushions ensure that there is a smaller probability of the particles passing through the cushions, which in turn ensures the cushion growth. The subsequent incoming granular jets provide positive feedback to the growth of the cushions behind the crowns. The cushions contribute to the blockage of particles and enhance the particle-particle interactions. Therefore, the average coordination and force chains exhibit rapid growth during this stage, as shown in Figs. 8e–8h. This indicates that the granular flows transition from a dilute flow state to a dense flow state. The kinetic energy of the granular flows is partly dissipated during the cushion growth. Moreover, jamming occurs between the baffles owing to the impedance effect. The kinetic energy of the granular flows is partly dissipated by the destruction and regeneration of the arches. During this stage, the crowns are considered as a type of deflecting dam and a type of barrier simultaneously.

At the steady flow state, the space between the rows of the baffle system is occupied by the blocked particles, as shown in Fig. 5i. The average coordination number reaches the peak value and complex force networks are formed during this stage, as shown in Fig. 8l. The high average coordination number indicates that the granular flows are in a dense flow state and impose a more effective restriction on the particle movement. The rearrangement of the entire force networks leads to the dissipation of flow energy. Granular flows with low kinetic energy cause the attenuation of the deflecting effect, as shown in Fig. 6i. During this stage, the crowns serve as type of barrier.

4 COMPARISON WITH CONVENTIONAL BAFFLE SYSTEM

4.1 DEM Model Program

To investigate the effectiveness of the crown-like baffle system, three layouts, namely, the conventional baffle system, crown-like baffle system with square baffles, and crown-like baffle system with triangular baffles, were simulated to determine their ability of impeding the avalanche mobility.

The typically adopted avalanche geometric scheme (Li et al., 2020; Bi et al., 2018) is shown in Fig. 10. The upper end of the scheme includes a reservoir whose length, width, and height are denoted as a, b, and c, respectively. The slope angle and length of each region are denoted as α, β, $L1$, and $L2$, respectively; $L3$ is the distance between the front edge of the baffle system and the upper end of slope B. The main parameters of the geometric scheme are listed in Table 3.

To better reflect the dynamic behaviour of actual avalanches, carefully calibrated micromechanical parameters were used in this study (Wang et al., 2020c). We assumed that the baffle system was made of C30 concrete and had the same micromechanics as the avalanche material. The initial avalanche deposition was an assembly of 150 000 randomly distributed spherical particles. The particle radius was set to 0.2 m. The micromechanical parameters are listed in Table 4.
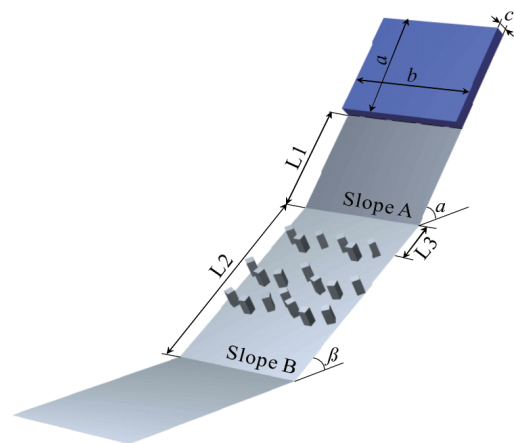

Figure 10. Geometry of idealized slope.

Table 3   Geometrical parameters of slope

Description	Symbol	Value
Avalanche length (m)	a	50
Avalanche width (m)	b	60
Avalanche depth (m)	c	6
Slope angle 1 (°)	α	50
Slope angle 2 (°)	β	30
Slope length 1 (m)	$L1$	60
Slope length 2 (m)	$L2$	100
Baffle distance (m)	$L3$	19

Table 4   Numerical parameters used in numerical experiments

Material	DEM paraments	Value	Source
Particle/path	Density ρ_1 (kg/m³)	2 600	Wang et al. (2020c)
	Poisson's ration υ_1	0.2	
	Shear modulus G_1 (MPa)	6 000	
	Friction coefficient μ_1	0.4	
	Rolling friction coefficient μ_{r1}	0.15	
Baffle	Density ρ_2 (kg/m³)	2 500	Code for design of concrete structures (2010)
	Poisson's ration υ_2	0.2	
	Elastic modulus G_2 (GPa)	30	
	Friction coefficient μ_2	0.4	Wang et al. (2020c)
	Rolling friction coefficient μ_{r2}	0.15	
Restitution coefficient e		0.4	Wang et al. (2020c)

The conventional baffle system was used as the baseline to demonstrate the effectiveness of the proposed crown-like baffle system. The conventional baffle system was configured based on the optimal parameters proposed by Ng et al. (2015) and Law et al. (2016), as shown in Fig. 11a. The square baffle, which has a width of 3.5 m, was used in this scheme. The baffle was set to 8 m, which is 1.5 times taller than the flow depth. The transverse blockage was set to 40%, which has been considered as the upper bound of this structure by various studies (Law et al., 2016; Choi et al., 2014). The design parameters of the conventional baffle system are listed in Table 5. The same baffle type was adopted in the scheme of the crown-like baffle system with square baffles, as shown in Fig. 11b. The third scheme is the crown-like baffle system with triangular baffles, as shown in Fig. 11c. To ensure that the baffle cross-sections have similar rigidity, the side length of the triangle was set to 5.0 m. The design parameters of the two crown-like baffle systems are listed in Table 6. The baffles were simulated using the wall element and were not breakable. In this paper, only the relationship between the energy dissipation and the different baffle layouts is discussed. Finally, monitoring sections were set to better evaluate the energy dissipation capacity of the different crown-like baffle systems, as shown in Fig. 11.

4.2 Cost-Effectiveness Analysis

As particles flowed past the baffle system, the energy was partly dissipated. Particles with residual kinetic energy were monitored by the monitoring section outlet, which was placed just downstream of the different baffle system layouts, respectively. Figure 12 shows the residual kinetic energy of the particles with different baffle system layouts. As can be seen, in the case of the conventional baffle system, the kinetic energy

reached 3.03 MJ at 9.04 s. Compared with the conventional baffle system, the peak kinetic energy values are obviously smaller with the crown-like baffle system. In the case of the crown-like baffle system with triangular baffles, the kinetic energy reached 2.90 MJ at 10.87 s. In the case of the crown-like baffle system with square baffles, the kinetic energy reached 2.54 MJ at 10.6 s. To better evaluate the energy dissipation capacity, we calculated the cumulative residual kinetic energy within the monitoring section outlet, which is defined as follows

$$E_r = \sum_{t=0}^{t=\text{end}} E_K^t \tag{14}$$

where E_r is the cumulative residual kinetic energy within the monitoring section, and E_K^t is the kinetic energy of the particles encompassed in the monitoring section at a given time. The calculation results are presented in Table 7.

Table 5   Design parameters of conventional baffle system

Name	Value (m)
Horizontal baffle length	3.5
Vertical baffle length	8
Baffle column spacing	5.25
Baffle row spacing	15.75

Table 6   Design parameters of crown-like baffle systems

Row number	Crown-like baffle system with square baffles			Crown-like baffle system with triangle baffles		
	r (m)	θ (°)	γ (°)	r (m)	θ (°)	γ (°)
R1	7.2	99	0	7.0	110	0
R2	13.0	61	12	15.6	84	3
R3	12.0	68	3	13.5	236	0

Table 7   Comparison of cumulative residual kinetic energy and concrete consumption in different cases

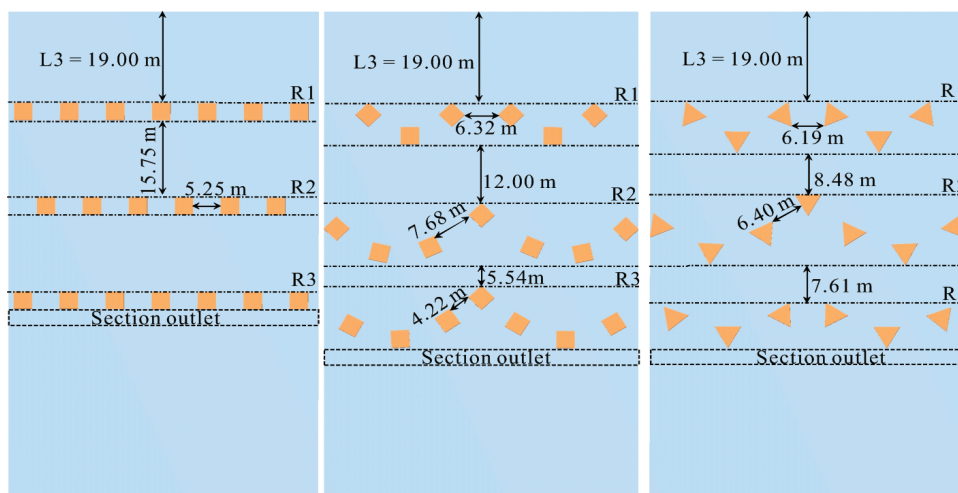| Baffle layout	Cumulative residual kinetic energy E_r (MJ)	Concrete consumption (m³)
Conventional baffle system	419.6	1 960.0
Crown-like baffle system with square baffles	340.9	1 960.0
Crown-like baffle system with triangle baffles	393.5	1 645.4

Figure 11. Layout of different baffle systems. (a) Conventional baffle system; (b) crown-like baffle system with square baffles; (c) crown-like baffle system with triangular baffles.
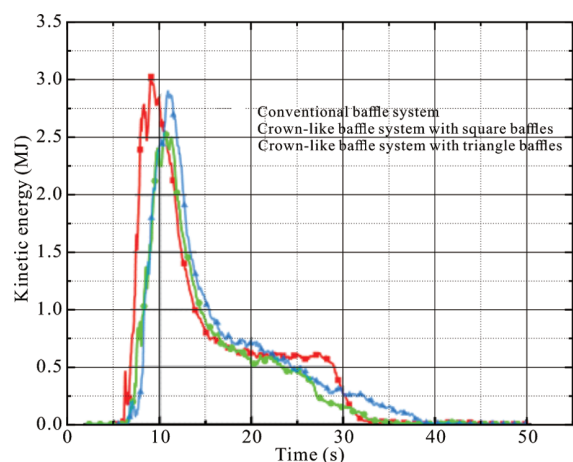
Figure 12. Evolution of kinetic energy of particles encompassed in each monitoring section outlet.

As shown in Table 7, the two layouts of the crown-like baffle system have better energy dissipation capability compared with the conventional baffle system. The cumulative residual kinetic energy of the crown-like baffle system with square baffles was reduced by 18.75% compared with the conventional baffle system with the same concrete consumption. In the case of the crown-like baffle system with triangular baffles, the cumulative residual kinetic energy was reduced by 6.22% with 83.94% of the concrete consumption of the conventional baffle system.

5   CONCLUSION

In this paper, a crown-like baffle system is proposed and compared with the conventional baffle system. The energy dissipation mechanism and cost-effectiveness of the crown-like baffle system were analysed using the DEM. The conclusions drawn from this study are as follows:

(1) More than 90% of the kinetic energy of granular flow is dissipated by particle-particle interactions. The function of the crown-like system is to enhance the particle-particle interaction.

(2) Two effects, namely, the impedance effect and deflection effect can be identified when the particles interact with the crown of the baffle system. The impedance effect appears when the particles collide with the baffles at a small incident angle. The deflection effect appears when the granular flow collides with the baffle at a large incident angle and the granular flow is deflected to flow parallel to the baffles.

(3) Under the impedance effect, arches form behind the first row of the baffle system. The interaction between the subsequent incoming granular flows with arches leads to the deceleration of the granular jets that form through the silts within the crowns. The interaction process is divided into three stages, namely, the cushion formation stage, cushion growth stage, and steady flow stage, when the granular flows pass through the second and the third row of the baffle system. The crowns play different roles at different stages of the interaction process.

(4) At the cushion formation stage, the granular jets are deflected to flow parallel to the baffles and form a cushion behind the crown. At the cushion growth stage, the subsequent incoming granular jets provide positive feedback to the cushion growth behind the crowns. The cushions help the blockage of particles and enhance the particle-particle interactions. At the cushion growth stage, the space between the rows of the baffle system is occupied by blocked particles. The rearrangement of the entire force networks leads to flow energy dissipation.

(5) Compared with the conventional baffle system, the crown-like baffle system has better energy dissipation capacity with the same or lower concrete consumption.

Accordingly, the concept of a crown-like baffle system with good energy dissipation capacity and cost-efficiency has good potential for use in mountain disaster prevention applications.

The design of conventional baffle system is relatively simple and have been successfully implemented in some mountainous areas. When the design parameters could meet the design requirements, the conventional baffle system may be a more convenient solution. However, when the design parameters of the conventional baffle system reach the upper limits and still cannot meet the design requirements, the crown-like baffle system may show its advantages in energy dissipation capacity and cost-efficiency.

The primary objective of this study is to investigate the energy dissipation mechanism and energy dissipation capacity using the DEM. However, exceptional design is required to realize the implementation of the proposed system in efficient disaster prevention measures. Therefore, the influence of the design parameters and flow characteristics on the energy dissipation capacity must be investigated in future work to facilitate the optimal design of the proposed structure.

REFERENCES CITED

Bi, Y. Z., Du, Y. J., He, S. M., et al., 2018. Numerical Analysis of Effect of Baffle Configuration on Impact Force Exerted from Rock Avalanches. *Landslides*, 15(5): 1029–1043. https://doi. org/10.1007/s10346-018-097 9-z

Choi, C. E., Cui, Y., Liu, L. H. D., et al., 2017. Impact Mechanisms of Granular Flow Against Curved Barriers. *Géotechnique Letters*, 7(4): 330–338. https://doi.org/10.1680/jgele.17.00068

Choi, C. E., Ng, C. W. W., Song, D., et al., 2014. Flume Investigation of Landslide Debris‒Resisting Baffles. *Canadian Geotechnical Journal*, 51(5): 540–553. https://doi.org/10.1139/cgj-2013-0115

Choi, C. E., Ng, C. W. W., Law, R. P. H., et al., 2015. Computational Investigation of Baffle Configuration on Impedance of Channelized Debris Flow. *Canadian Geotechnical Journal*, 52(2): 182–197. https://doi.org/10.1139/cgj-2013-0157

Choi, C. E., Ng, C. W. W., Goodwin, G. R., et al., 2016. Flume Investigation of the Influence of Rigid Barrier Deflector Angle on Dry Granular Overflow Mechanisms. *Canadian Geotechnical Journal*, 53 (10): 1751–1759. https://doi.org/10.1139/cgj-2015-0248

Dang, B. L., Nguyen-Ngoc, H., Hoang, T. D., et al., 2019. Numerical Investigation of Novel Prefabricated Hollow Concrete Blocks for Stepped-Type Seawall Structures. *Engineering Structures*, 198: 109558. https://doi.org/10.1016/j.engstruct.2019.109558

Daoud, M., Williams, C. E., 1999. Soft Matter Physics. Springer, Berlin. 320

Delannay, R., Valance, A., Mangeney, A., et al., 2017. Granular and Particle-Laden Flows: From Laboratory Experiments to Field Observations. *Journal of Physics D*: *Applied Physics*, 50(5): 053001. https://doi.org/10.1088/1361-6463/50/5/053001

DEM Solutions (2020) EDEM 2020.1 Document. Edinburgh

Fei, J. B., Jie, Y. X., Sun, X. H., et al., 2020. Experimental Investigation on Granular Flow Past Baffle Piles and Numerical Simulation Using a M (I)-Rheology-Based Approach. *Powder Technology*, 359: 36–46. https://doi.org/10.1016/j.powtec.2019.09.069

Goodwin, S. R., Choi, C. E., 2020. Slit Structures: Fundamental Mechanisms of Mechanical Trapping of Granular Flows. *Computers and Geotechnics*, 119: 103376. https://doi.org/10.1016/j.compgeo.2019.103376

van der Gucht, J., 2018. Grand Challenges in Soft Matter Physics. *Frontiers in Physics*, 6: 6–8. https://doi.org/10.3389/fphy.2018.00087

Hu, M. B., Liu, Q. Y., Jiang, R., et al., 2015. Phase Transition and Flow-Rate Behavior of Merging Granular Flows. *Physical Review E*, *Statistical*, *Nonlinear*, *and Soft Matter Physics*, 91(2): 022206. https://doi.org/10.1103/physreve.91.022206

Huang, Y., Zhang, B., Zhu, C. Q., 2021. Computational Assessment of Baffle Performance Against Rapid Granular Flows. *Landslides*, 18(1): 485–501. https://doi.org/10.1007/s10346-020-01511-6

Hungr, O., Evans, S. G., Bovis, M. J., et al., 2001. A Review of the Classification of Landslides of the Flow Type. *Environmental and Engineering Geoscience*, 7(3): 221–238. https://doi.org/10.2113/gseegeosci.7.3.221

Jiang, Y. J., Fan, X. Y., Li, T. H., et al., 2018. Influence of Particle-Size Segregation on the Impact of Dry Granular Flow. *Powder Technology*, 340: 39–51. https://doi.org/10.1016/j.powtec.2018.09.014

Jiang, Y. J., Towhata, I., 2013. Experimental Study of Dry Granular Flow and Impact Behavior Against a Rigid Retaining Wall. *Rock Mechanics and Rock Engineering*, 46(4): 713–729. https://doi.org/10.1007/s00603-012-0293-3

Khan, A., Verma, S., Hankare, P., et al., 2020. Shock-Shock Interactions in Granular Flows. *Journal of Fluid Mechanics*, 884: 1–13. https://doi.org/10.1017/jfm.2019.988

Kwan, J. S. H., Koo, R. C. H., Ng, C. W. W., 2015. Landslide Mobility Analysis for Design of Multiple Debris-Resisting Barriers. *Canadian Geotechnical Journal*, 52(9): 1345–1359. https://doi.org/10.1139/cgj-2014-0152

Law, R. P. H., Choi, C. E., Ng, C. W. W., 2016. Discrete-Element Investigation of Influence of Granular Debris Flow Baffles on Rigid Barrier Impact. *Canadian Geotechnical Journal*, 53(1): 179–185. https://doi.org/10.1139/cgj-2014-0394

Li, X. P., Yan, Q. W., Zhao, S. X., et al., 2020. Investigation of Influence of Baffles on Landslide Debris Mobility by 3D Material Point Method. *Landslides*, 17(5): 1129–1143. https://doi.org/10.1007/s10346-020-01346-1

Mancarella, D., Hungr, O., 2010. Analysis of Run-up of Granular Avalanches Against Steep, Adverse Slopes and Protective Barriers. *Canadian Geotechnical Journal*, 47(8): 827–841. https://doi.org/10.1139/t09-143

Matthew R. K., 2017. Granular Geomechanics. Elsevier, 274

Mead, S. R., Cleary, P. W., 2015. Validation of DEM Prediction for Granular Avalanches on Irregular Terrain. *Journal of Geophysical Research*: *Earth Surface*, 120(9): 1724–1742. https://doi.org/10.1002/2014jf003331

MOHURD (Ministry of Housing and Urban-Rural Development of the People's Republic of China), 2010. GB 50010-2010: Code for design of concrete structures. SAC, Beijing, China (in Chinese)

Ng, C. W. W., Choi, C. E., Kwan, J. S. H., et al., 2014. Effects of Baffle Transverse Blockage on Landslide Debris Impedance. *Procedia Earth and Planetary Science*, 9: 3–13. https://doi.org/10.1016/j.proeps.2014.06.012

Ng, C. W. W., Choi, C. E., Song, D., et al., 2015. Physical Modeling of Baffles Influence on Landslide Debris Mobility. *Landslides*, 12(1): 1–18. https://doi.org/10.1007/s10346-014-0476-y

Ng, C. W. W., Choi, C. E., Goodwin, S. R., et al., 2017. Interaction between Dry Granular Flow and Deflectors. *Landslides*, 14(4): 1375–1387. https://doi.org/10.1007/s10346-016-0794-3

Salciarini, D., Tamagnini, C., Conversini, P., 2010. Discrete Element Modeling of Debris-Avalanche Impact on Earthfill Barriers. *Physics and Chemistry of the Earth*, *Parts A/B/C*, 35(3/4/5): 172–181. https://doi.org/10.1016/j.pce.2009.05.002

Shen, W. G., Zhao, T., Zhao, J. D., et al., 2018. Quantifying the Impact of Dry Debris Flow Against a Rigid Barrier by DEM Analyses. *Engineering Geology*, 241: 86–96. https://doi.org/10.1016/j.engge o.2018.05.011

Sosio, R., Crosta, G. B., Hungr, O., 2008. Complete Dynamic Modeling Calibration for the Thurwieser Rock Avalanche (Italian Central Alps). *Engineering Geology*, 100(1/2): 11–26. https://doi.org/10.1016/j.enggeo.2008.02.012

Suda, J., Strauss, A., Rudolf-Miklau, F., et al., 2009. Safety Assessment of Barrier Structures. *Structure and Infrastructure Engineering*, 5(4): 311–324. https://doi.org/10.1080/15732470701189498

Tiago, P., Júlio, E., 2010. Case Study: Damage of an RC Building after a Landslide—Inspection, Analysis and Retrofitting. *Engineering Structures*, 32(7): 1814–1820. https://doi.org/10.1016/j.engstruct.2010.02.018

Wang, D. P., Li, Q. Z., Bi, Y. Z., et al., 2020. Effects of New Baffles System under the Impact of Rock Avalanches. *Engineering Geology*, 264: 105261. https://doi.org/10.1016/j.enggeo.2019.105261

Wang, D. P., Li, Q. Z., Bi, Y. Z., et al., 2020b. Optimal Layout of a New Type of Baffle Based on High-Risk Areas of Rock Avalanches. *Rock and Soil Mechanics*, 41(4): 1323–1365 (in Chinese with English Abstract)

Wang, W. P., Yin, Y. P., Yang, L. W., et al., 2020. Investigation and Dynamic Analysis of the Catastrophic Rockslide Avalanche at Xinmo, Maoxian, after the Wenchuan M_s 8.0 Earthquake. *Bulletin of Engineering Geology and the Environment*, 79(1): 495–512. https://doi.org/10.1007/s10064-019-01557-4

Zhang, L. R., Nguyen, N. G. H., Lambert, S., et al., 2017. The Role of Force Chains in Granular Materials: From Statics to Dynamics. *European Journal of Environmental and Civil Engineering*, 21(7/8): 874–895. https://doi.org/10.1080/19648189.2016.1194332

Zhang, X., Wang, X. Y., Chen, W. S., et al., 2021. Numerical Study of Rockfall Impact on Bridge Piers and Its Effect on the Safe Operation of High-Speed Trains. *Structure and Infrastructure Engineering*, 17(1): 1–19. https://doi.org/10.1080/15732479.2020.1730406

Zhao, Y. D., Shi, Y., Wu, F. H., 2020. Preliminary Analyses of a Catastrophic Rock Avalanche that Occurred in Ganluo County, Sichuan Province, China. *Landslides*, 17(6): 1515–1517. https://doi.org/10.1007/s10346-020-01412-8

Zhou, G. G. D., Du, J. H., Song, D. R., et al., 2020. Numerical Study of Granular Debris Flow Run-up Against Slit Dams by Discrete Element Method. *Landslides*, 17(3): 585–595. https://doi.org/10.1007/s10346-019-01287-4